IEEE Access
Multidisciplinary | Rapid Review | Open Access Journal

Received August 1, 2021, accepted August 23, 2021, date of publication August 25, 2021, date of current version September 3, 2021.

Digital Object Identifier 10.1109/ACCESS.2021.3107906

Self-Learning in Aerial Robotics Using type-2 Fuzzy Systems: Case Study in Hovering Quadrotor Flight Control

AYAD AL-MAHTURI[1], (Student Member, IEEE), FENDY SANTOSO[1,2], (Senior Member, IEEE), MATTHEW A. GARRATT[1], (Senior Member, IEEE), AND SREENATHA G. ANAVATTI[1]

[1]School of Engineering and Information Technology, University of New South Wales, Canberra, ACT 2612, Australia
[2]Defence and Systems Institute (DASI), Science, Technology, Engineering, Mathematics (STEM), University of South Australia, Adelaide, SA 5095, Australia

Corresponding author: Ayad Al-Mahturi (ayad.almahturi@gmail.com)

This work was supported by the Australian Government Research Training Program Scholarship.

ABSTRACT This paper aims to design an enhanced self-adaptive interval type-2 fuzzy control system (ESAF2C) for stabilization of a quadcopter drone under external disturbances. Due to the ability to accommodate the *footprint-of-uncertainty* (FoU), an interval type-2 Takagi-Sugeno fuzzy scheme is employed to directly address the uncertainties in the nonlinear system. Sliding mode control (SMC) is utilized to optimize the upper and lower parameters of our proposed ESAF2C system using a self-tuning technique. The 'Enhanced Iterative Algorithm with Stop Condition' type-reducer is accommodated in the proposed design for its suitability to real-time implementation. To handle external disturbances and the ground effect in the closed-loop flight control system, a robustness term is added to the control effort. Lyapunov theory is applied to prove the stability of our closed loop control system. Moreover, we study the measurement noise effect for different levels of noise powers using our proposed technique. The efficacy of the proposed controller is investigated in a hovering quadcopter drone through numerical simulations and real-time flight tests in the presence of external disturbances. We highlight the disturbance rejection capability of our proposed control system with respect to type-1 fuzzy and conventional PID controllers.

INDEX TERMS Interval type-2 fuzzy control, disturbance rejection, UAV, Lyapunov stability, real-time flight tests.

I. INTRODUCTION

Drones, a prominent nickname for unmanned aerial vehicles (UAVs), have been attracting a large amount of consideration in the last few decades. They have been used in a myriad of applications (e.g. transportation [1], inspection of power transmission lines [2], search and rescue missions [3], and collecting traffic information [4]. They are already having a major impact in both military and civilian applications [1]. One major benefit of multirotor UAVs is their capability to hover, to perform vertical take-off and landing (VTOL), and to fly in confined spaces (see Fig. 1) [5]–[10]. Besides, Small multi-rotor UAVs are frequently used because of their small size, ease of maintenance, and adaptability for dangerous environments, which also makes them appropriate for research purposes [11], [12]. However, this sort of aircraft is difficult to control throughout the full flight envelope due to various types of uncertainties, as well as to its complex and nonlinear characteristics [6], [13].

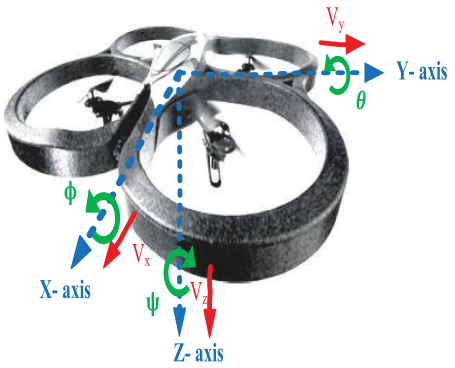

FIGURE 1. The body-frame $\{B\}$ of a Parrot AR.Drone, where (θ, ϕ, ψ) represents the rotation along *xyz*-axes respectively.

Many robotic systems are dynamically unstable, nonlinear, and are multi-input multi-output (MIMO) systems, and

The associate editor coordinating the review of this manuscript and approving it for publication was Venkateshkumar M.

therefore, robust control systems are required to stabilize them [14]. The classical model-based control approaches such proportional integral-derivative (PID) [15], linear quadratic regulator (LQR) [16], and model predictive controllers (MPC) [17] can provide optimal control performance when the model is well-defined, precise and there are no external uncertainties. Nevertheless, there are inevitable uncertainties in aerial robots, (e.g. lack of modeling, mechanical wear, rotor damage, battery drain and sensor and actuator faults [18], [19]). Another aerodynamic challenge when flying a rotorcraft vehicle at a reasonably low altitude is ground effect, which occurs due to the distortion of rotor downwash due to the ground obstruction [20], [21]. This phenomenon leads to a limited ability to obtain a precise flight control system. In other words, the ground effect brings significant nonlinearity (altering the thrust characteristic) and uncertainties into the closed-loop control system [21]. In the face of the aforementioned uncertainties, the control performance of conventional methods becomes poor [22]. In other words, designing a reliable closed-loop control system is a challenging task in the face of uncertainties [23].

In general, adaptive control methods have proven to be more effective than fixed gain controllers [14], [22], [24], [25]. Intelligent control systems such as fuzzy logic controllers (FLCs), artificial neural networks (ANNs) controllers, and their combinations have been extensively employed to control nonlinear systems with complex dynamics [26]–[30]. Under the umbrella of FLCs, Takagi-Sugeno (TS) fuzzy control systems have several advantages. Among them, TS fuzzy systems allow description of a nonlinear system via a set of local linear system domains with corresponding well-designed membership functions (MFs) [31]–[33]. Moreover, FLCs have the ability to represent uncertainties in nonlinear systems by their continuous MFs, where their membership degree is between the interval [0, 1] [34].

Nevertheless, since uncertainty information is not incorporated in the membership function of type-1 fuzzy sets (T1-FSs), controlling nonlinear systems subjected to uncertainties cannot be handled precisely. In other words, parameter uncertainties in nonlinear systems may lead to uncertain membership degree, and hence, type-1 fuzzy scheme becomes more conservative [35]. Hence, type-2 fuzzy logic systems (T2FLSs) were proposed in [36] based on type-2 fuzzy sets (T2-FSs) to handle such uncertainties captured by their type-2 fuzzy membership functions. The membership functions of IT2FSs are three dimensional, where a new parameter called the *footprint-of-uncertainties* (FoU) is introduced [14], [37]. Besides, a type-reduction (TR) process is required to convert between type-1 and type-2 fuzzy sets before carrying out the defuzzification process [9]. In the fuzzy literature, there are various TR techniques (e.g. the well-known Karnik-Mendel (KM) algorithm, center-of-sets, centroid, and other methods [34], [38], [39]). Although there are several studies of multirotor drone control based FLCs, most of these studies are based on T1-FLCs.

Moreover, because of the computational complexity in the TR process for converting T2-FSs into T1-FSs, type-2 fuzzy logic controller systems (T2FLCs) are rarely employed in real-time applications [34]. As a result, to reduce the computational burden of the generalised T2FLCs while maintaining the major advantages of type-2 fuzzy system, interval type-2 fuzzy logic control systems (IT2FLCs) were proposed, where the secondary grade variables of a T2-FSs are defined as one. IT2FLCs are used to speed up the response to uncertain input for membership functions, allowing more flexibility in designing the desired control law and providing the capacity to handle additional uncertainties commonly found in nonlinear systems [14], [40].

II. RELATED WORK

Since IT2FLCs provide an extra degree of freedom to handle uncertainties in nonlinear systems, they have been applied for navigating quadcopter UAVs. In [9], IT2FLCs were proposed for quadcopter altitude control, where good results were achieved. Nevertheless, the fuzzy parameters were tuned manually. Manual tuning of FLCs can be a time-consuming, inefficient, and tedious task [41]. There are several previous studies where IT2FLCs have been combined with sliding mode control (SMC), resulting in uncertainties compensation, and improvement of the overall control performance by canceling the chattering effect on SMC control systems [42]. In [41], an IT2FLC based SMC theory was proposed for a quadcopter UAV (QUAV), achieving reasonably good control performance compared to a T1-FLC and conventional PID controllers. However, the fuzzy control law was designed as a combination of both an IT2FLC system and a PID controller, resulting in extra effort for tuning PID parameters. Similarly, in [43], a hybrid IT2FLC-based PID controller was proposed for a power system, where the fuzzy parameters were tuned using the firefly algorithm-particle swarm optimization technique. Nevertheless, their proposed representation requires extra tuning for its PID parameters. In the work by [44], a fault-tolerant control based on interval type-2 fuzzy neural networks and sliding mode controller was developed for a 6-DOF octocopter UAV. Although their proposed controller has the ability to guarantee the stability of the proposed control system, it lacks experimental validation. Furthermore, IT2FLC parameters are reduced to type-1 fuzzy sets in most of the practical IT2FLC applications, resulting in similar behavior to T1-FLCs, as the *FOU* is not explicitly included in the fuzzy design. Lastly, there is a lack of real-time experiments using IT2FLCs.

Motivated by the aforementioned observation, the contribution of this paper can be highlighted as follows:

- A novel stand-alone enhanced self-adaptive interval type-2 fuzzy controller named the *ESAF2C* is proposed for position control of a hovering QUAV, whose type-2 fuzzy parameters are tuned online using the sliding mode control theory, making the system robust to variations in system parameters and external disturbance.

Unlike most of the state-of-the-art work in literature, the chattering phenomenon is eliminated by smoothing out the control discontinuity around the sliding surface. The 'Enhanced Iterative Algorithm with Stop Condition' (EIASC) type-reducer is accommodated in designing the ESAF2C, which is more suitable for real-time implementation than other type-reducers for its computational efficiency.

- We investigate the robustness of the proposed controller in the face of external disturbances (e.g. ground effects, wind gust, measurement noise) and perform a rigorous comparative study with respect to T1-FLC and conventional counterparts, where our research findings demonstrate an improved disturbance rejection using our proposed ESAF2C. Moreover, our proposed closed-loop control system proves its ability to filter measurement noise as investigated in our simulation.
- We conduct real-time flight tests for a hovering QUAV under stochastic wind disturbances to validate the efficacy of our theoretical claims. Specifically, we investigate the control performance in the face of external wind disturbance, using an industrial fan in the hover mode. Our findings show that the proposed control technique has the capability to learn its parameters in an online manner and to handle external stochastic wind gust disturbance better than T1-FLC and conventional PID counterparts.
- The stability analysis of our proposed control system is investigated using the Lyapunov theory.

This paper is organized as follows: Section III presents background materials on IT2FLCs. Section IV introduces the nonlinear dynamic model of the QUAV. Section V explains the proposed control scheme. Section VI analyzes the simulation results, while Section VII describes the experimental results. Finally, Section VIII draws conclusions.

III. OVERVIEW OF type-2 FUZZY CONTROLLER

A. OVERVIEW OF type-2 FUZZY SETS

Let us define a type-2 fuzzy set (T2FSs), represented by $\tilde{A}$, which consist of $((x,u),\mu_{\tilde{A}}(x,u))$, where for every $x \in X$, there is a primary membership function u in which $u \in J_x$, and a secondary membership function $\mu_{\tilde{A}}(x,u)$). T2FSs can be expressed mathematically as follows [34]:

$$\begin{aligned}\tilde{A} &= ((x,u),\mu_{\tilde{A}}(x,u))|\forall x \in X, |\forall u \in J_x \subseteq [0,1],\\ &= \mu_{\tilde{A}}(x,u) \subseteq [0,1]\end{aligned} \tag{1}$$

B. OVERVIEW OF INTERVAL type-2 FUZZY SETS

To minimize the computational burden of T2FSs, interval type-2 fuzzy sets (IT2FSs) are introduced, where the secondary MFs are equal to 1 [34]. IT2FSs have gained popularity due to the compact structures used to accommodate the FoUs, which allows greater freedom in designing a closed-loop control system and higher suitability for real-time applications. IT2FSs can be expressed mathematically as follows:

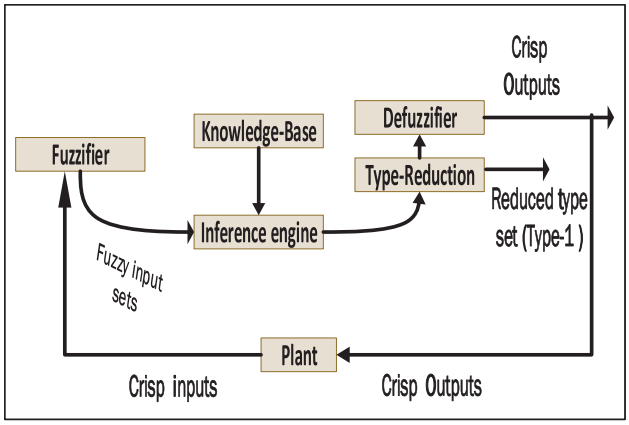

FIGURE 2. type-2 fuzzy logic system representation.

$$\begin{aligned}\tilde{A} &= ((x,u),1)|\forall x \in X, |\forall u \in J_x \subseteq [0,1]\\ &= \sum_{x\in X}\sum_{u\in J_x}((x,u),1)\end{aligned} \tag{2}$$

C. INTERVAL type-2 FUZZY CONTROLLER STRUCTURE

Interval type-2 fuzzy controller comprises of four major elements, namely, fuzzifier, rule base fuzzy system, type reduction and defuzzifier as shown in Fig. 2. The function of each block is explained as follows:

1) **Fuzzifier**: the fuzzifier block transforms the crisp input vector $\mathbf{X} = [e_1, e_2, \ldots, e_3]^T$ into a type-2 fuzzy set $\tilde{A}$. In this block, each input is represented by an IT2FS using trapezoidal MFs. The reason for choosing trapezoidal MFs is that their analytical structure is easy to derive [12]. In IT2FLC, MFs provide a three-dimensional (3D) representation, which combine the upper membership function (UMF) and the lower membership function (LMF) as shown in Fig. 3. The upper and the lower IT2-trapezoidal MFs can be represented as follows [45]:

$$\underline{\mu}_{\tilde{F}}(x) = \begin{cases} 0, & x \le \hat{m}-\hat{a} or x > \hat{m}+\hat{a}\\ w\dfrac{x-\hat{m}+\hat{a}}{\hat{a}-\hat{c}}, & \hat{m}-\hat{a} < x \le \hat{m}-\hat{c}\\ w, & \hat{m}-\hat{c} < x \le \hat{m}+\hat{c}\\ w\dfrac{\hat{m}+\hat{a}-x}{\hat{a}-\hat{c}} & \hat{m}+\hat{c} < x \le \hat{m}+\hat{a}\end{cases} \tag{3}$$

$$\overline{\mu}_{\tilde{F}}(x) = \begin{cases} 0, & x \le \hat{m}-\hat{b} or x > \hat{m}+\hat{b}\\ \dfrac{x-\hat{m}+\hat{b}}{\hat{b}-\hat{d}}, & \hat{m}-\hat{b} < x \le \hat{m}-\hat{d}\\ 1, & \hat{m}-\hat{d} < x \le \hat{m}+\hat{d}\\ \dfrac{\hat{m}+\hat{b}-x}{\hat{b}-\hat{d}} & \hat{m}+\hat{d} < x \le \hat{m}+\hat{b},\end{cases} \tag{4}$$

where $\hat{a}$, $\hat{b}$, $\hat{c}$, $\hat{d}$ and w are constrained. To simplify our design and for the sake of real-time implementation,

TABLE 1. X-control fuzzy rules representation.

Rules	Inputs		Outputs	
	e_x	$\dot{e}_x$	x position	
r_1	N	N	$\upsilon_1^l = \upsilon_{01}^l + \upsilon_{11}^l e_x + \upsilon_{21}^l \dot{e}_x$	$\upsilon_1^r = \upsilon_{01}^r + \upsilon_{11}^r e_x + \upsilon_{21}^r \dot{e}_x$
r_2	N	Z	$\upsilon_2^l = \upsilon_{02}^l + \upsilon_{12}^l e_x + \upsilon_{22}^l \dot{e}_x$	$\upsilon_2^r = \upsilon_{02}^r + \upsilon_{12}^r e_x + \upsilon_{22}^r \dot{e}_x$
r_3	N	P	$\upsilon_3^l = \upsilon_{03}^l + \upsilon_{13}^l e_x + \upsilon_{23}^l \dot{e}_x$	$\upsilon_3^r = \upsilon_{03}^r + \upsilon_{13}^r e_x + \upsilon_{23}^r \dot{e}_x$
r_4	Z	N	$\upsilon_4^l = \upsilon_{04}^l + \upsilon_{14}^l e_x + \upsilon_{24}^l \dot{e}_x$	$\upsilon_4^r = \upsilon_{04}^r + \upsilon_{14}^r e_x + \upsilon_{24}^r \dot{e}_x$
r_5	Z	Z	$\upsilon_5^l = \upsilon_{05}^l + \upsilon_{15}^l e_x + \upsilon_{25}^l \dot{e}_x$	$\upsilon_5^r = \upsilon_{05}^r + \upsilon_{15}^r e_x + \upsilon_{25}^r \dot{e}_x$
r_6	Z	P	$\upsilon_6^l = \upsilon_{06}^l + \upsilon_{16}^l e_x + \upsilon_{26}^l \dot{e}_x$	$\upsilon_6^r = \upsilon_{06}^r + \upsilon_{16}^r e_x + \upsilon_{26}^r \dot{e}_x$
r_7	P	N	$\upsilon_7^l = \upsilon_{07}^l + \upsilon_{17}^l e_x + \upsilon_{27}^l \dot{e}_x$	$\upsilon_7^r = \upsilon_{07}^r + \upsilon_{17}^r e_x + \upsilon_{27}^r \dot{e}_x$
r_8	P	Z	$\upsilon_8^l = \upsilon_{08}^l + \upsilon_{18}^l e_x + \upsilon_{28}^l \dot{e}_x$	$\upsilon_8^r = \upsilon_{08}^r + \upsilon_{18}^r e_x + \upsilon_{28}^r \dot{e}_x$
r_9	P	P	$\upsilon_9^l = \upsilon_{09}^l + \upsilon_{19}^l e_x + \upsilon_{29}^l \dot{e}_x$	$\upsilon_9^r = \upsilon_{09}^r + \upsilon_{19}^r e_x + \upsilon_{29}^r \dot{e}_x$

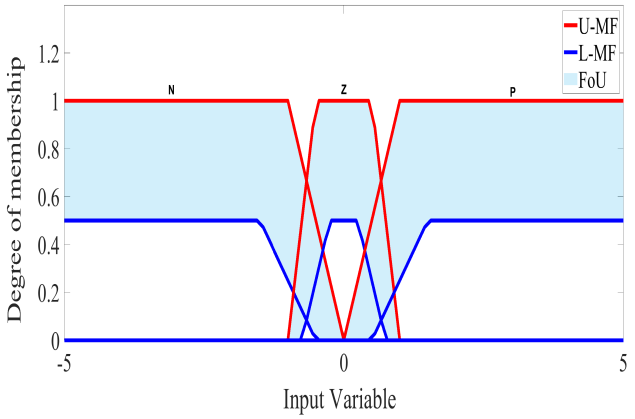

FIGURE 3. General interval type-2 trapezoidal membership function.

we set $\hat{a} = \hat{b}$, $\hat{c} = 0$, $w = 1$. Hence, there are only three free parameters to be tuned.

2) **Fuzzy Rules**: rules representation of IT2-FLCs is the same as T1-FLCs counterpart. A fuzzy inference rule can be expressed as follows:

$$\begin{aligned} &IF\ e_1\ is\ \tilde{F}_1^i\ and\ e_2\ is\ \tilde{F}_2^i\ and\ e_n\ is\ \tilde{F}_n^i, \\ &THEN\ Y^i = [\upsilon_i^l\ \upsilon_i^r], \end{aligned} \tag{5}$$

where e_n represents an input variable; $\tilde{F}_{ni}$ labels IT2-FSs antecedents; Y^i denotes the output of the i^{th} rule base; and υ_i^l and υ_i^r express the lower and upper consequent parameters, respectively. In our work, we utilized nine rules. The interpretation of these rules can be shown in Table 1, where N means negative, Z denotes zero, and P represents positive.

3) **Firing interval block**: for IT2FLCs, the firing level is represented by a firing interval. This process can be achieved using the minimum (t-*norm*) operation. The firing interval can be calculated as follows:

$$\begin{aligned} F^i(x_1, \ldots, x_n) &= [\underline{f}^i(x_1, \ldots, x_n), \overline{f}^i(x_1, \ldots, x_n)] \\ &= [\underline{f}^i, \overline{f}^i]. \end{aligned} \tag{6}$$

The expressions for $\underline{f}^i$ and $\overline{f}^i$ are given as follows:

$$\underline{f}_i = \prod_{i=1}^{n} \underline{\mu}_{\tilde{F}_n^i}, \qquad \overline{f}_i = \prod_{i=1}^{n} \overline{\mu}_{\tilde{F}_n^i}. \tag{7}$$

4) **Type-reduction**: the type-reduction process maps IT2FSs to T1FSs in order to get a crisp output. In our work, a center-of-sets type-reduction [34] is used as follows:

$$Y_{cos} = [y_l,\ y_r], \tag{8}$$

where y_l and y_r are represented as:

$$y_l = \frac{\sum_{i=1}^{L} c_l \overline{f} + \sum_{i=L+1}^{M} c_l \underline{f}}{\sum_{i=1}^{L} \overline{f} + \sum_{i=L+1}^{M} \underline{f}} \tag{9}$$

$$y_r = \frac{\sum_{i=1}^{R} c_r \underline{f} + \sum_{i=R+1}^{M} c_r \overline{f}}{\sum_{i=1}^{R} \underline{f} + \sum_{i=R+1}^{M} \overline{f}}. \tag{10}$$

In the above equation, L and R are called the switching points and are computed using the EIASC algorithm [34]. EIASC algorithm has been found faster than the widely used KM type-reducer [34].

5) **Defuzzifier**: the last process is to obtain the defuzzified outputs. The final output y is calculated as follows:

$$y = (y_l + y_r)/2. \tag{11}$$

IV. QUAV DYNAMIC MODEL

QUAVs have six degrees of freedom (DOF), with high mobility and four rotors. The motion of a QUAV can be expressed by the following twelve state variables, namely,

$$\vec{x} = [X, Y, Z, \dot{X}, \dot{Y}, \dot{Z}, \theta, \phi, \psi, p, q, r]^T, \tag{12}$$

where $[X, Y, Z]^T$ represents the linear positions in the inertial frame $\{A\}$; $[\dot{X}, \dot{Y}, \dot{Z}]^T$ denotes the linear velocities across the xyz-axes; $[\theta, \phi, \psi]^T$ are the three Euler's angles, namely, the pitch, roll and yaw, respectively; $[p, q, r]^T$ denotes the angular rates in the body frame $\{B\}$ of the QUAV (see Fig. 4). The total thrust and moments for the four control inputs on each control axis can be described as follows:

$$\vec{U} = [U_1, U_2, U_3, U_4]^T = \left[T_{\sum}, M_1, M_2, M_3\right]^T, \tag{13}$$

where $\vec{U}$ represents control variables; $T_{\sum} = \sum_{i=1}^{N} T_i$ is the total sum of thrusts along $\{B\}$; and $M_{1,2,3}$ denote the moments

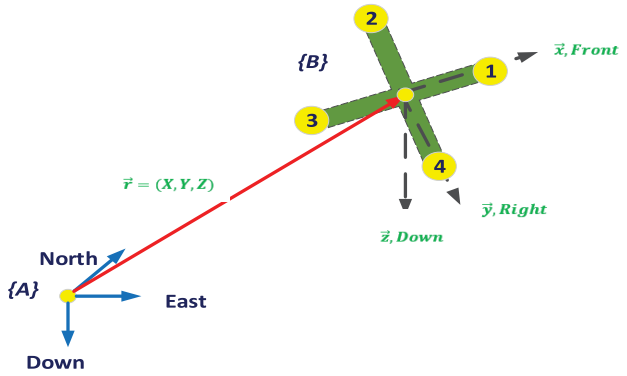

FIGURE 4. Coordinate frame of a QUAV.

generated by N number of rotors [46]. In the case of our QUAV, $N = 4$, hence the angular speed of each rotor can be described as:

$$\begin{bmatrix} T_\sum \\ M_1 \\ M_2 \\ M_3 \end{bmatrix} = \begin{bmatrix} 1 & 1 & 1 & 1 \\ 0 & l & 0 & -l \\ l & 0 & -l & 0 \\ \frac{K_q}{K_T} & \frac{-K_q}{K_T} & \frac{K_q}{K_T} & \frac{-K_q}{K_T} \end{bmatrix} \begin{bmatrix} T_1 \\ T_2 \\ T_3 \\ T_4 \end{bmatrix} \quad (14)$$

where $T_{1,2,3,4}$ are the thrust from each individual motor; K_q $[kg.m^2]$ represents the lumped rotor torque coefficient; K_T $[kg.m]$ denotes the lumped rotor thrust coefficient; and l $[m]$ is the arm length. Finally, the equations of motion can be summarized as follows:

$$\begin{cases} \ddot{X} = -(\sin\psi \sin\phi + \cos\psi \sin\theta \cos\phi)\frac{T_\sum}{m} \\ \ddot{Y} = -(-\cos\psi \sin\phi + \sin\psi \sin\theta \cos\phi)\frac{T_\sum}{m} \\ \ddot{Z} = g - (\cos\theta \cos\phi)\frac{T_\sum}{m} \\ \dot{p} = \frac{I_{yy} - I_{zz}}{I_{xx}} \cdot qr + \frac{1}{I_{xx}} \cdot M_1 \\ \dot{q} = \frac{I_{zz} - I_{xx}}{I_{yy}} \cdot rp + \frac{1}{I_{yy}} \cdot M_2 \\ \dot{r} = \frac{I_{xx} - I_{yy}}{I_{zz}} \cdot pq + \frac{1}{I_{zz}} \cdot M_3, \end{cases} \quad (15)$$

where $I_{xx,yy,zz}$ represent the moment of inertia on the xyz-axes. The detailed physical parameters of the QUAV and the meaning of each symbol can be found in [46]. Fig. 5 illustrates the position control structure for the QUAV.

V. PROBLEM FORMULATION

Consider a nonlinear dynamic system n^{th} order as

$$x^{(n)} = \bar{f}(\mathbf{x}, t) + \bar{b}(\mathbf{x}, t)u(t) + d(t), \quad (16)$$

where the state vector $\mathbf{x}$ can be represented as $\mathbf{x} = \left[x\ \dot{x}\ \ldots\ x^{(n-1)}\right]^T$; $\bar{f}(\mathbf{x}, t)$ and $\bar{b}(\mathbf{x}, t)$ denote the state vector nonlinear functions; $u(t)$ represents the control input; and $d(t)$ expresses an external disturbance.

Considering the tracking error that is, the difference between the desired and the actual values as:

$$\mathbf{e} = \mathbf{x}_d - \mathbf{x} = \left[\, e(t) \quad \dot{e}(t) \quad \ldots \quad e(t)^{(n-1)} \,\right]^T, \quad (17)$$

where $\mathbf{x}_d = \left[x_d\ \dot{x}_d\ \ldots\ x_d^{(n-1)}\right]^T$ is the desired tracking values, and $\mathbf{x}$ is the actual value. Eq. (17) can be expanded as follows:

$$\begin{cases} \dot{e}_1 = e_2(t) \\ \dot{e}_2 = e_3(t) \\ \quad \vdots \\ \dot{e}_n(t) = \dot{\mathbf{x}}_{dn} - \bar{f}(\mathbf{x}, t) - \bar{b}(\boldsymbol{x}, t)u(t) - d(t) \end{cases} \quad (18)$$

Remark 1: Practically, it is difficult to measure all state variables of the system. Hence, our study selects two major control variables, named, the error $e(t)$ and its derivative $\dot{e}(t)$.

A. DESIGN OF SLIDING SURFACE

Remark 2: The design of SMC consists of two stages: 1) design of the reaching phase, and 2) design of a sliding surface phase. Such control technique employs a discontinuous control law that has the ability to drive the system to a specified sliding surface $S(t)$, and also to preserve its motion along $S(t)$ [27], [47].

A sliding surface $S(e, t) = 0$ can be defined as follows:

$$S(t) = \delta e(t) + \dot{e}(t), \quad (19)$$

where δ is a strictly positive constant. For theoretical study, it is appropriate to assume the nonlinear terms in (16) are known. This case, however, may not true in real life. But that is when the idea of robust control comes to picture i.e. to deal with uncertainties. Hence, the control law $u_{final}(t)$ can be constructed as follows [14]:

$$u_{final}(t) = \bar{b}(\mathbf{x}, t)^{-1}[\dot{\mathbf{x}}_{dn}(t) - \bar{f}(\mathbf{x}, t) - \dot{e}_n(t) + \dot{S}(t) + \delta S(t)]. \quad (20)$$

The inputs to the proposed fuzzy controller are the $e(t)$ and $\dot{e}(t)$. Moreover, for producing the control signal $u(t)$ in 16, fuzzy operations are deployed to approximate the equivalent control law $u_{final}(t)$. It is worth mentioning that the purpose of using SMC is to derive the dynamics of the system so that $S(t) = \delta e(t) + \dot{e}(t) = 0$. By following the equivalent control law $u_{final}(t)$ and by considering the sliding surface and its derivative as the inputs to the fuzzy control system, the system is asymptotically stable [48], so that $\delta S(t) + \dot{S}(t) = 0$.

The convergence of $S(t)$ and $\dot{S}(t)$ to zero is guaranteed as δ is always a positive number. Likewise, the convergence of $e(t)$ and $\dot{e}(t)$ to zero is always guaranteed according to the definition in (19). To avoid the complexity of model-based computations, this study utilized fuzzy system capability to map between the input variables and the control law $u(t)$. In our case, the control input might have differences from the optimal control law $u_{final}(t)$. Hence, using Eqs. (18) and (20), the following equation can be derived as

$$\dot{S}(t) = \bar{b}(\mathbf{x}, t)[u_{final}(t) - u(t)] - \delta S(t). \quad (21)$$

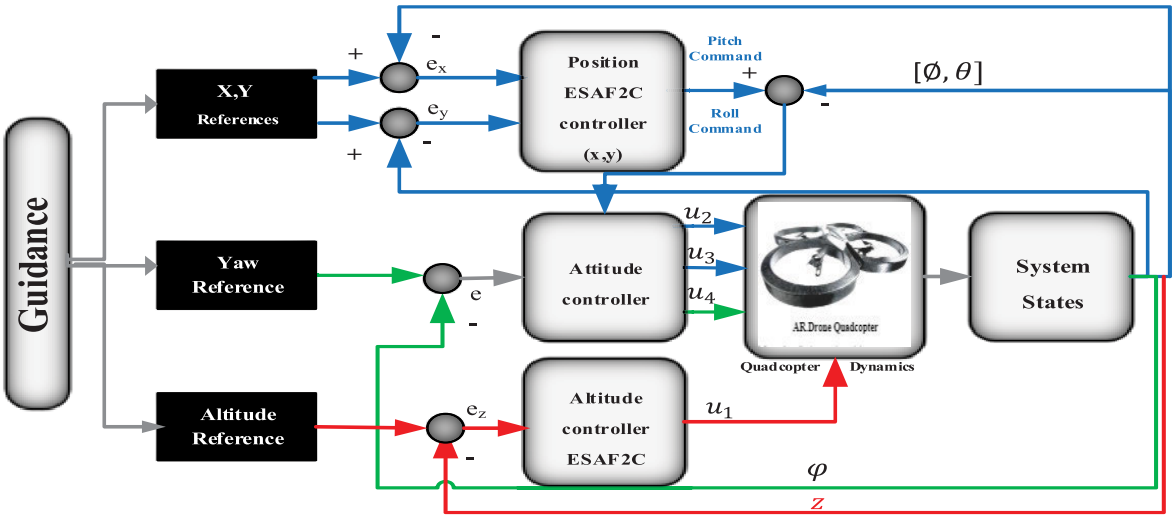

FIGURE 5. Control structure based on ESAF2C for position tracking of a nonlinear quadcopter plant, where we employ the attitudes and the thrust to create a position control loop outside the velocity loop of the Parrot AR.Drone.

By multiplying (21) with $S(t)$, it yields to:

$$\dot{S}(t)S(t) = S(t)\left(\overline{b}(\mathbf{x}, t)[u_{final}(t) - u(t)] - \delta S(t)\right) \quad (22)$$

Following the Lyapunov theory leads to $\dot{S}(t)S(t) < 0$, which represent the reaching phase of the sliding surface. Therefore, the purpose of our study is to design a control signal $u(t)$ that satisfies the reaching condition to guarantee the convergence of the overall control system.

To obtain a robust control performance against system dynamics uncertainties, a discontinuous term is added to the final control part across the sliding surface $S(t)$. In other words, the discontinuous term act as a robustness term, and can be added as the reaching control element of the control effort [49]. The discontinuous term can be represented as:

$$u_{robust} = \beta(t)sgn(S(t)), \quad (23)$$

where β denotes a design parameter and *sgn* represents the *signum* function, which can be defined as follows:

$$sgn(S(t)) = \begin{cases} 1, & if\ S(t) > 0 \\ 0, & if\ S(t) = 0 \\ -1, & if\ S(t) < 0 \end{cases} \quad (24)$$

Nevertheless, employing the *signum* function causes a chattering phenomenon. One way to eliminate the chattering phenomenon is by smoothing out the continuity of the *signum* function and employing a smooth function such as *sat* or *tanh*. In our design, we use the *sat* function, which can be expressed as follows [50]:

$$sat\left(\frac{S}{\iota}\right) = \begin{cases} \frac{S}{\iota}, & if\ |S| \le |\iota| \\ sgn(S), & otherwise \end{cases} \quad (25)$$

where ι is a design factor representing the thickness of the boundary layer. Finally, the constructed control law considering uncertainties can be written as:

$$u(t) = u_{final}(t) + u_{robust}(t), \quad (26)$$

where $u_{robust}(t) = \beta(t)sat(S(t)/\iota)$.

B. ESAF2C ADAPTIVE LAW

The proposed adaptation law for the ESAF2C is obtained using the gradient descent method, that is to minimize the $S(t)\dot{S}(t)$ with respect to υ^l and υ^r in (5). The proposed structure can be depicted in Fig. 6. Hence, the modified υ^l and υ^r can be expressed as follows:

$$\begin{cases} \upsilon^l_{t+1} = \upsilon^l(t) - \Lambda \dfrac{\partial S(t)\dot{S}(t)}{\partial \upsilon^l(t)} \\ \upsilon^r_{t+1} = \upsilon^r(t) - \Lambda \dfrac{\partial S(t)\dot{S}(t)}{\partial \upsilon^r(t)}, \end{cases} \quad (27)$$

where Λ is a design adaptive parameter and $[\upsilon^l,\ \upsilon^r]$ are the consequent fuzzy parameters. By applying the chain rule, (27) can be rewritten as:

$$\begin{cases} \upsilon^l_{t+1} = \upsilon^l(t) - \Lambda \dfrac{\partial S(t)\dot{S}(t)}{\partial u(t)} \dfrac{\partial u(t)}{\partial \upsilon^l(t)} \\ \qquad = \upsilon^l(t) + \Lambda \overline{b}(\mathbf{x}, t)S(t) \dfrac{\partial u(t)}{\partial \upsilon^l(t)}. \\ \upsilon^r_{t+1} = \upsilon^r(t) - \Lambda \dfrac{\partial S(t)\dot{S}(t)}{\partial u(t)} \dfrac{\partial u(t)}{\partial \upsilon^r(t)} \\ \qquad = \upsilon^r(t) + \Lambda \overline{b}(\mathbf{x}, t)S(t) \dfrac{\partial u(t)}{\partial \upsilon^r_{(}t)}. \end{cases} \quad (28)$$

To simplify (28) further, we combine the design adaptive parameter Λ with the overall system input parameter $\overline{b}(\mathbf{x}, t)$ as a learning parameter, λ, [14], [51]. Therefore, for the sake of practical implementation, the adaptive law with respect to

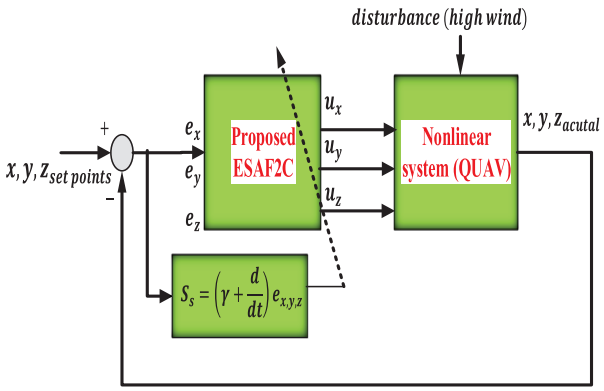

FIGURE 6. Proposed ESAF2C structure for QUAV control, where u_x, u_y, u_z represent the control signals for xyz-axes, respectively.

the firing strength can be rewritten as follows:

$$\begin{cases} \upsilon_{t+1}^{l} = \upsilon^{l}(t) + \lambda S(t) \left(\dfrac{\underline{f}^{i}(t))}{\sum_{l=1}^{m} \left(\overline{f}^{i}(t) + \underline{f}^{i}(t) \right)} \right) \\ \upsilon_{t+1}^{r} = \upsilon^{r}(t) + \lambda S(t) \left(\dfrac{\overline{f}^{i}(t))}{\sum_{l=1}^{m} \left(\overline{f}^{i}(t) + \underline{f}^{i}(t) \right)} \right). \end{cases} \tag{29}$$

In the work by [52], [53], a dead-zone concept was introduced to reduce the drift effect of the fuzzy consequents. Hence, the modified equations for updating the consequent parameters can be rewritten in (30), as shown at the bottom of the next page, where κ is a design parameter >0; and ι is the thickness of the boundary layer as discussed in (25).

C. STABILITY ANALYSIS

In this section, we study the stability of our proposed ESAF2C using the Lyapunov theory.

Lemma 5.1: [14] If optimal upper and lower consequent parameters υ^{l} and υ^{r} exist, which lead to the control law $\tilde{u}$, the final approximate of the control law $\mathbf{u}_{final}(t)$ has bounded error of ζ, that leads to:

$$max|\tilde{u}(\mathbf{x}, \bar{\upsilon}) - \mathbf{u}_{final}(x)| < \zeta, \tag{31}$$

where $\tilde{u}(\mathbf{x}, \overline{\upsilon}) = \overline{\upsilon}^{T}\mathbf{W}$; $\mathbf{u}_{final}(t)(x) = \overline{\upsilon}^{T}\mathbf{W} + \zeta$; $\boldsymbol{W} = [W_l, W_r] = \left[\frac{\underline{f}^{i}(t))}{\sum_{l=1}^{m}\left(\overline{f}^{i}(t)+\underline{f}^{i}(t)\right)}, \frac{\overline{f}^{i}(t))}{\sum_{l=1}^{m}\left(\overline{f}^{i}(t)+\underline{f}^{i}(t)\right)} \right]$ and $\bar{\upsilon} = \left[\bar{\upsilon}^{l}, \bar{\upsilon}^{r}\right]$.

If we describe $\bar{\upsilon} = \overline{\upsilon} - \tilde{\upsilon}$, which can be defined as the difference between the desired and actual consequent, we can rewrite (21) as:

$$\dot{S}(t) = \bar{b}[\bar{\upsilon}^{T}\mathbf{W} + \zeta] - \delta S(t). \tag{32}$$

This study chose the Lyapunov function as follows:

$$V = \frac{1}{2}s_{\nabla}^{2} + \frac{\bar{b}}{2\lambda}\bar{\upsilon}^{T}\bar{\upsilon}, \quad \lambda \neq 0, \tag{33}$$

where $s_{\nabla} \equiv S - \iota \bullet sat(S/\iota)$ and ι denotes the thickness of boundary layer [48].

By differentiating (33) with respect to time, it leads to:

$$\begin{cases} = s_{\nabla}\dot{s}_{\nabla} + \dfrac{\bar{b}}{\lambda}\bar{\upsilon}^{T}\dot{\bar{\upsilon}} + \dfrac{\dot{\bar{b}}}{2\lambda}\bar{\upsilon}^{T}\bar{\upsilon} \\ = s_{\nabla}\dot{s}_{\nabla} + \dfrac{\bar{b}}{\lambda}\bar{\upsilon}^{T}\left[\dot{\overline{\upsilon}} - \dot{\tilde{\upsilon}}\right] + \dfrac{\dot{\bar{b}}}{2\lambda}\bar{\upsilon}^{T}\bar{\upsilon} \\ = s_{\nabla}\left[-\delta s + \bar{b}\left(\bar{\upsilon}^{T}\mathbf{W} + \zeta\right)\right] \\ -\bar{b}\bar{\upsilon}^{T}\left(s_{\nabla}\mathbf{W} - \dfrac{\kappa}{\lambda}|s_{\nabla}|\tilde{\upsilon}\right) + \dfrac{\dot{\bar{b}}}{2\lambda}\bar{\upsilon}^{T}\bar{\upsilon} \\ \dot{V} = s_{\nabla}\left[-\delta(s_{\nabla} + \iota) + \bar{b}\zeta\right] + \dfrac{\bar{b}}{\lambda}\kappa|s_{\nabla}|\bar{\upsilon}^{T}\tilde{\upsilon} + \dfrac{\dot{\bar{b}}}{2\lambda}\bar{\upsilon}^{T}\bar{\upsilon} \\ \leq |s_{\nabla}|\left(-\delta|s_{\nabla}| - \delta\iota + \bar{b}\zeta - \dfrac{1}{\lambda}\bar{b}\kappa\bar{\upsilon}^{T}\bar{\upsilon}\right. \\ \left. + \dfrac{1}{\lambda}\bar{b}\kappa|\bar{\upsilon}||\overline{\upsilon}|\right) + \dfrac{\dot{\bar{b}}}{2\lambda}\bar{\upsilon}^{T}\bar{\upsilon} \\ = -|s_{\nabla}|\Theta - \dfrac{1}{\lambda}\left[|s_{\nabla}|\bar{b}\kappa - \dfrac{\dot{\bar{b}}}{2}\right]\bar{\upsilon}^{T}\bar{\upsilon}, \end{cases} \tag{34}$$

where $\Theta = \delta\iota + \delta|s_{\nabla}| - \bar{b}\left(\zeta + \frac{1}{\lambda}\kappa|\bar{\upsilon}||\overline{\upsilon}|\right)$.

Following the work in [14], choosing suitable parameters for ι and κ for $\Theta > 0$, (34) indicates that $\dot{V} < 0$ at any time that $s_{\nabla} \notin R \equiv \{|s_{\nabla}| < (\frac{\dot{\bar{b}}}{2\kappa\bar{b}\lambda})\}$. Therefore, the stability of the control system is guaranteed based on the Lyapunov theory.

VI. SIMULATION RESULTS

In this section, we study the efficacy of our proposed adaptive control system in stabilizing the QUAV. We examine the performance of our proposed ESAF2C in the presence of external disturbances and measurement noise while tracking various reference signals along the (xyz)-axes. We compare our proposed method with a conventional PID controller and both T1-FLC and IT2FLC counterparts. The performance indices such as the root mean square error (RMSE), rising time (t_r), and settling time (t_s) are reported in this section. RMSE values can be calculated using (35).

$$\mathbf{RMSE} = \sqrt{\frac{\sum_{k=1}^{N}(y_{actual} - \hat{y}_k)^2}{N}} \tag{35}$$

where y_{actual} is model actual output, $\hat{y}_k$ represents the estimated fuzzy output.

We utilized a trapezoidal MF for the fuzzification and the TS-type fuzzy model for the consequent parameters process. We employed nine rules, with three membership functions for each input. The inputs to the proposed fuzzy controllers are the error and its derivative in the range between $[-5, 5]$ as shown in Fig. 3. The sliding surface parameters were chosen as: $\delta_x = 0.8, \delta_y = 0.7, \delta_z = 1.1$. The consequent parameters started learning from scratch and were initialized with zeros. Moreover, the added artificial gust has the following parameters: gust velocity $= 2m/s$; gust amplitude $= 5m$; for xyz-axes.

A. CASE 1: NOMINAL CONDITION

First, a step reference was fed as the desired trajectory at a hovering point of $[0.7, 0.8, 1]$ m for xyz-axes respectively. For the altitude position, the set-point was increased to 1.2 m after 5 sec. A better control system performance was obtained using our proposed ESAF2C compared to T1-fuzzy and T2-fuzzy counterparts, while comparable performance to a conventional PID controller in the case of nominal condition as shown in Fig. 7. Besides, we performed the analysis with different reference signals (e.g., sine wave signal), where better closed-loop control performance was observed using our proposed method compared to other controllers as shown in Fig. 8. The tracking errors and the control efforts throughout the experiment are shown in Fig. 9 and Fig. 10, demonstrating a favorable performance using the ESAF2C.

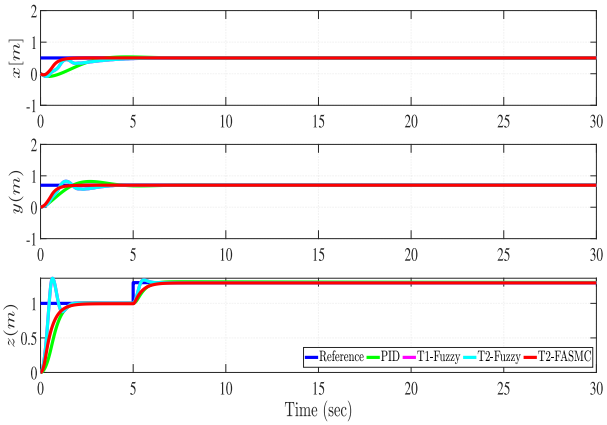

FIGURE 7. Simulation results for position control in the *xyz*-axes for different controllers on the nominal system (step input).

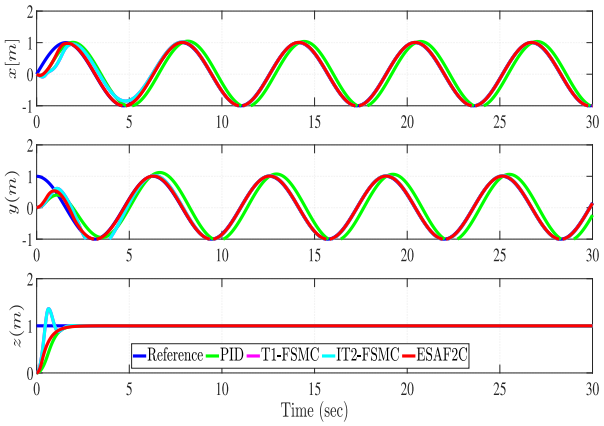

FIGURE 8. Simulation results for position control in the *xyz*-axes for different controllers on the nominal system (sine input).

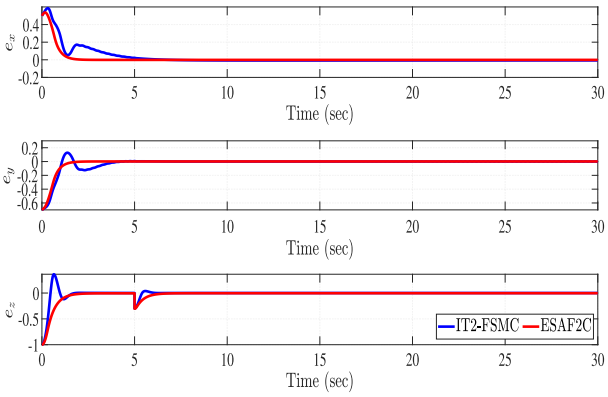

FIGURE 9. Simulation results for the error signals for IT2-FSMC and ESAF2C on the nominal system.

B. CASE 2: DISTURBANCE CONDITION

For further investigation of our purposed technique, we added artificial stochastic wind/gust disturbance. As can be seen in Figs. 11 & 12, the conventional PID controller failed to stabilize the system in the presence of disturbances, while a stable performance was observed using our proposed technique. For more visualization, the dotted squares and dotted circles in Figs. 11, 12, 13 are presented, which demonstrate the improvement of our proposed technique compared to the other controllers. The proposed ESAF2C performed better than their type-1 and type-2 fuzzy counterparts as indicated by its lower error values shown in Fig. 13 and Table. 2. Moreover, as can be seen in Fig. 14, the chattering effect was eliminated using our proposed ESAF2C by adopting the *saturation* function to smooth out the chattering control discontinuity of the sliding surface.

C. CASE 3: SENSOR MEASUREMENT NOISE EFFECT

For further investigation of robustness, feedback band-limited white noises with various noise powers were added to the sensor data, while having the stochastic artificial winds present. In other words, the noise was added to the position signals

$$\begin{cases} \upsilon^l_{t+1} = 0, & \text{if } S \le \iota \\ \upsilon^r_{t+1} = 0, & \text{if } S \le \iota \\ \upsilon^l_{t+1} = \kappa |S| \upsilon^l(t) + \lambda S(t) \left(\dfrac{\underline{f}^i(t))}{\sum_{l=1}^{m} \left(\overline{f}^i(t) + \underline{f}^i(t) \right)} \right), & \text{if } S > \iota \\ \upsilon^r_{t+1} = \kappa |S| \upsilon^r(t) + \lambda S(t) \left(\dfrac{\overline{f}^i(t))}{\sum_{l=1}^{m} \left(\overline{f}^i(t) + \underline{f}^i(t) \right)} \right), & \text{if } S > \iota \end{cases} \tag{30}$$

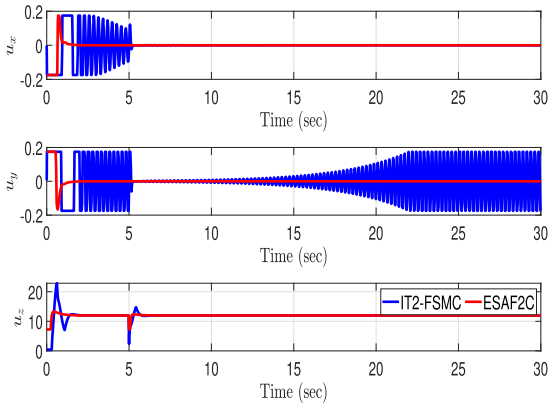

FIGURE 10. Simulation results for the control signals for IT2-FSMC and ESAF2C on the nominal system.

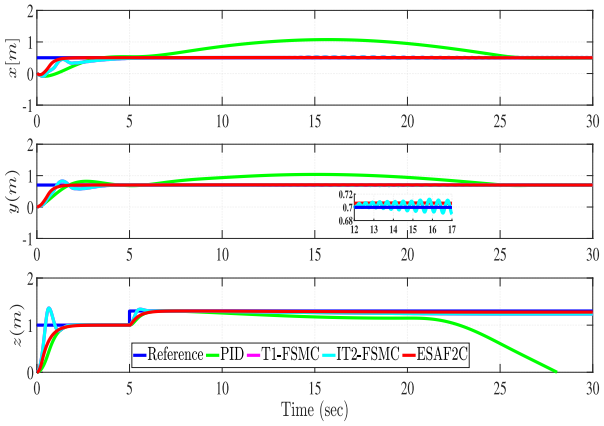

FIGURE 11. Simulation results for different controllers for position control in the *xyz*-axes under disturbances (step input).

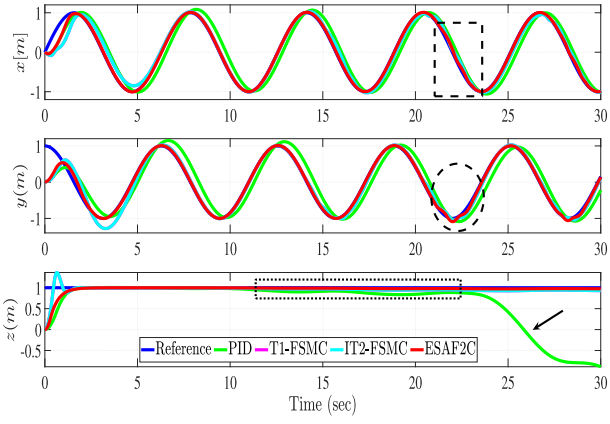

FIGURE 12. Simulation results for different controllers for position control in the *xyz*-axes under disturbances (Sine input).

(x, y, z). As shown in 15, our proposed controller proved its robustness and ability to handle noisy sensor data efficiently compared to T1-FSMC and IT2-FSMC counterparts.

D. COMPUTATIONAL LOAD

The quantification of the computation load was evaluated under Core i7-10750H CPU @ 2.6GHz with 16.0 GB of RAM, which was collected using the *tic* and *toc* MATLAB

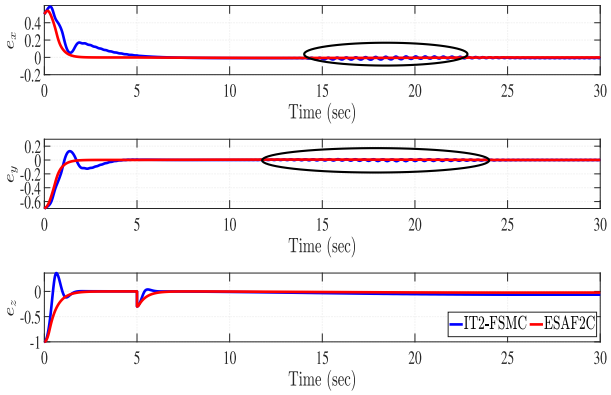

FIGURE 13. Simulation results for the error signals for IT2-FSMC and ESAF2C under uncertainties.

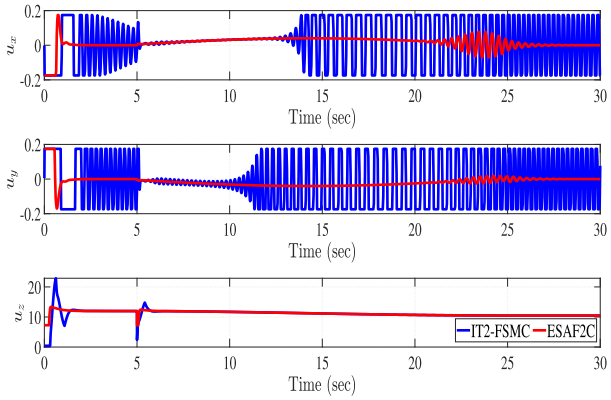

FIGURE 14. Simulation results for the control signals for IT2-FSMC and ESAF2C under uncertainties.

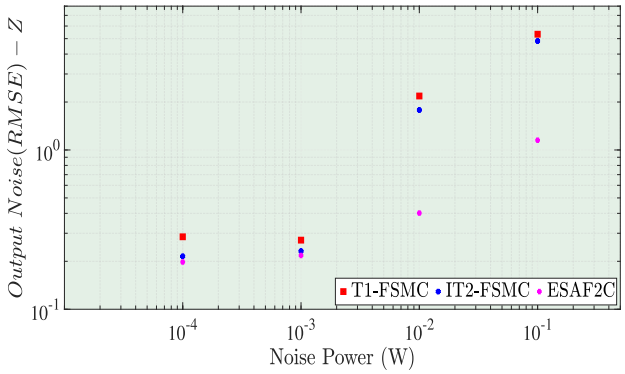

FIGURE 15. Measurement noise effect (comparison between ESAF2C, IT2-FSMC and T1-FSMC), *Z*-position control.

functions. The sampling time $= 0.01sec$ and the simulation time is $30sec$. Table 3 illustrates that the computation cost for the proposed method is higher than the PID and the T1-FSMC controllers. Despite being more computationally expensive, the performance of our adaptive fuzzy ESAF2C is superior compared to benchmark controllers, especially in the face of uncertainty. Today, with current speed of computer, this burden should not be a problem as it was in the past.

VII. EXPERIMENTAL RESULTS

To investigate the practical capability of our proposed method, multiple real flight tests were conducted. The experiments were performed in our indoor flight test space, which

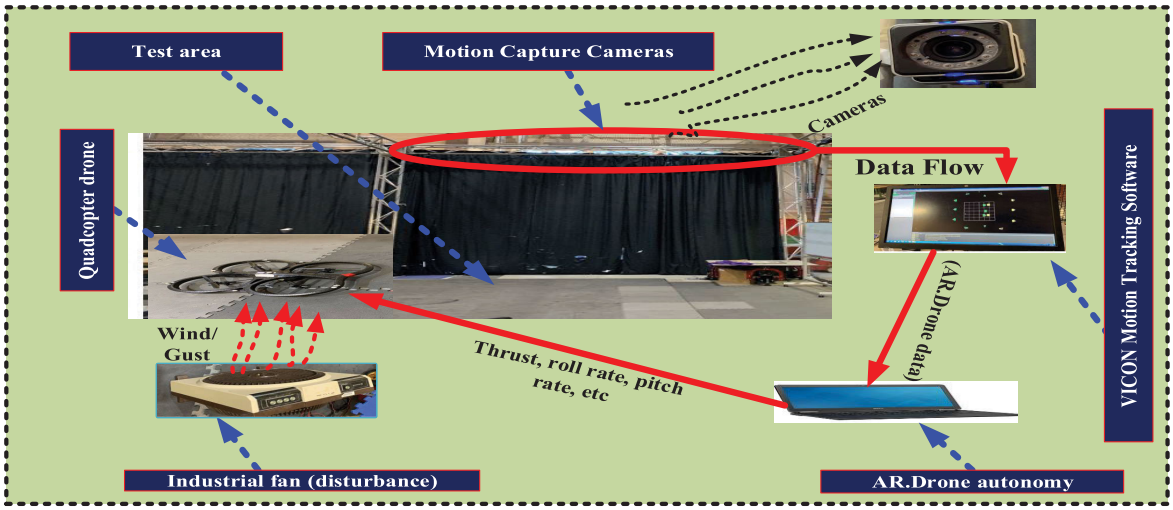

FIGURE 16. Data flow of the overall system architecture, demonstrating the information flow of our UAV including the position, orientation, velocity, acceleration, angular rates, etc.

TABLE 2. Simulation results for multiple controllers with disturbances.

$x-position$					
Metrics	**PID**	**T1-FSMC**	**IT2-FSMC**	**ESAF2C**	**Units**
t_r	0.78	3.63	3.52	1.79	(s)
t_s	25.92	17.85	15.85	2.35	(s)
$RMSE$	0.356	0.125	0.109	0.0721	(m)
$y-position$					
Metrics	**PID**	**T1-FSMC**	**IT2-FSMC**	**ESAF2C**	**Units**
t_r	1.26	21.52	20.56	5.86	(s)
t_s	24.36	3.89	3.85	2.593	(s)
$RMSE$	0.221	0.115	0.095	0.0833	(m)
$z-position$					
Metrics	**PID**	**T1-FSMC**	**IT2-FSMC**	**ESAF2C**	**Units**
t_r	1.52	4.12	4.08	3.25	(s)
t_s	29.81	16.42	14.25	5.84	(s)
$RMSE$	0.542	0.215	0.1152	0.1013	(m)

TABLE 3. Computation load for various controllers.

Control method	**Computational load** (sec)
PID	10.16
T1-FSMC	33.34
IT2-FSMC	56.46
ESAF2C	53.68

is equipped with 19 VICON motion capture cameras. These powerful cameras have the ability to track all motions of our QUAV. We utilize the VICON Motion Tracker software to analyze and store real-time flight data (e.g., position, velocity, Euler angles, acceleration, and angular rates). The QUAV can be controlled via WI-FI at a frequency of $100Hz$, thanks to the Robot Operating System (ROS) protocol. Besides, we utilized nine fuzzy rules and a trapezoidal MF for real-time implementation. Similar to the simulation study, the performance indices were reported in Table 4. Besides, we demonstrated the adaptation trajectory of the upper and the lower ESAF2C parameters during the flight tests. The experimental

TABLE 4. Experimental evaluation using three different controllers in hovering mode with high-wind disturbance.

$X-position$				
Metrics	**PID**	**T1-Fuzzy**	**ESAF2C**	**Units**
t_r	13.86	5.55	2.43	(s)
t_s	59.39	58.94	55.90	(s)
$RMSE$	0.1936	0.26	0.14	(m)
$Y-position$				
Metrics	**PID**	**T1-Fuzzy**	**ESAF2C**	**Units**
t_r	36.9	5.96	2.34	(s)
t_s	58.98	42.54	35.32	(s)
$RMSE$	0.30	0.23	0.19	(m)
$Z-position$				
Metrics	**PID**	**T1-Fuzzy**	**ESAF2C**	**Units**
t_r	4.0711	0.2479	0.1216	(s)
t_s	60.4351	58.9833	52.3981	(s)
$RMSE$	0.201	0.163	0.095	(m)

setup and the data flow of the overall system architecture can be demonstrated in Fig. 16.

A. CASE 1: NOMINAL CLOSED-LOOP POSITION CONTROL

We have conducted various experiments to control the (xyz) positions of our QUAV. As depicted in Fig. 17, the performance of three different controllers was compared. In this flight test, the desired set points were set to be $[0, 0, 1-1.2]m$ for xyz-axes, respectively. Fig. 17 shows a comparable performance of the PID and type-2 counterparts with respect to the proposed ESAF2C technique. Besides, shorter settling time was reported from the conventional PID controller, as our proposed ESAF2C requires time to adapt its parameters.

B. CASE 2: EXTERNAL DISTURBANCE CLOSED-LOOP POSITION CONTROL

To validate our theoretical study, we studied the performance under external disturbance. We utilized an industrial fan to act as a wind disturbance. Our experimental results indicated

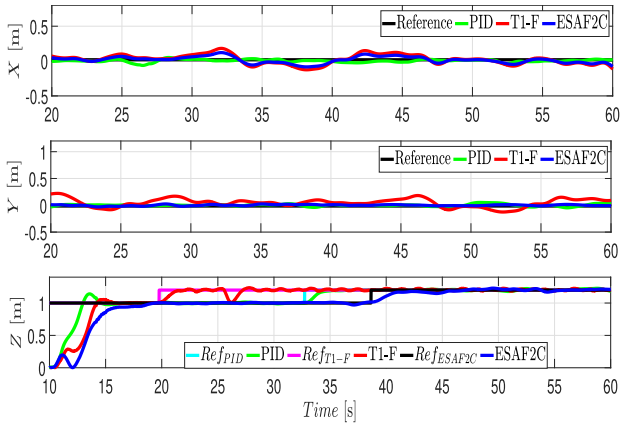

FIGURE 17. Output *xyz* positions of our QUAV during real-time flight tests (hover mode) for different controllers.

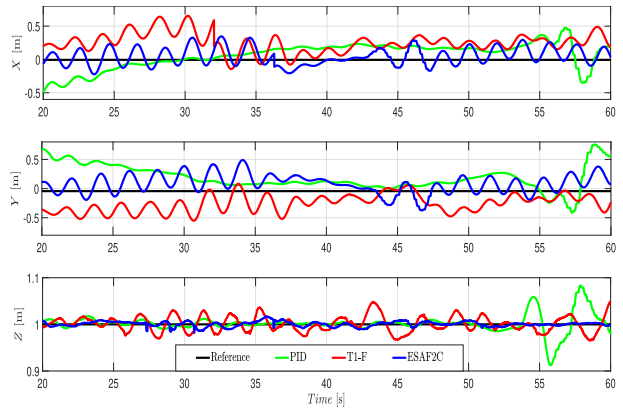

FIGURE 18. Output *xyz* positions under external disturbance during real-time flight tests (hover mode) for different controllers.

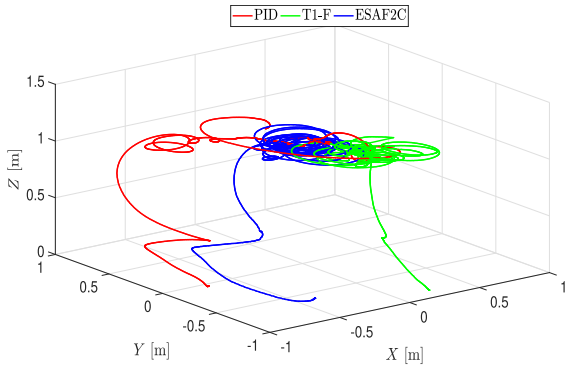

FIGURE 19. Output *xyz* positions under external disturbance during real-time flight tests (hover mode) in 3-D shape.

that the performance of our proposed ESAF2C is better than its type-1 fuzzy and conventional PID counterparts as shown in Figs. 18 & 19, thanks to the *FOU* in IT2FLCs, that incorporate uncertainties efficiently. The online learning of the upper and the lower ESAF2C parameters are plotted in Fig. 20. The fuzzy parameters were varying according to the amount of applied gusts. In other words, Fig. 20, shows the convergence of the six parameters. Moreover, it is worth mentioning that the upper and the lower parameters started learning from scratch, where they were initialized with zeros. Table 4 shows

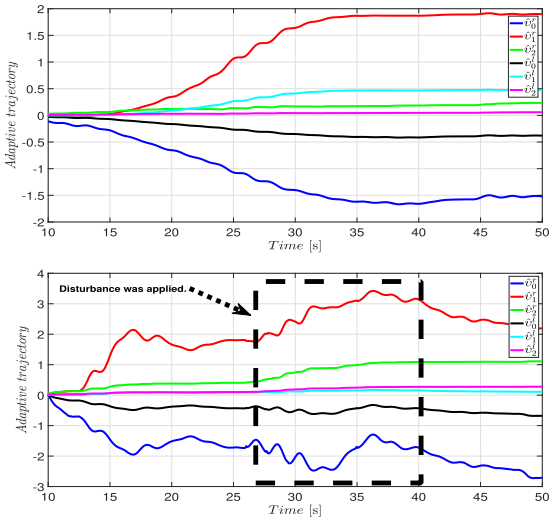

FIGURE 20. Upper figure shows the online parameters learning using ESAF2C in hover mode (nominal condition), lower figure shows online parameters learning using ESAF2C (under disturbance).

the experimental evaluation for three different controllers under external wind disturbance, where lower RMSE values were recorded using ESAF2C system.

VIII. CONCLUSION

In this paper, a novel ESAF2C controller was proposed to stabilize a quadcopter drone under external disturbances. On the basis of the SMC scheme, a self-tuning technique was implemented to tune SMC parameters, where SMC was utilized to tune fuzzy upper and lower variables. Our approach was validated using extensive numerical simulations and real-time flight tests. The proposed method was performed and implemented in the ROS environment. The stability analysis was examined using the Lyapunov theory. The proposed fuzzy control system approach can be considered a promising technique for the practical implementation of nonlinear systems. Our control scheme was computationally efficient as it requires only three membership functions, resulting in nine fuzzy rules only. Moreover, the proposed technique system demonstrated better control performance in the face of uncertainties (ground effects) and external disturbance (wind gusts) when compared to its type-1 fuzzy and conventional PID counterparts. Furthermore, our proposed closed-loop control system proved its ability to filter measurement noise that might occur during real-time implementation. We believe that the outcomes of this paper provided extra flexibility to fine-tune IT2FLCs and demonstrated the capability to implement IT2FLCs in real-time. For future work, the proposed control system can be implemented in multi-robot systems (e.g., swarm of drones).

REFERENCES

[1] D. Floreano and R. J. Wood, "Science, technology and the future of small autonomous drones," *Nature*, vol. 521, no. 7553, pp. 460–466, 2015.
[2] Y. Zhang, X. Yuan, W. Li, and S. Chen, "Automatic power line inspection using UAV images," *Remote Sens.*, vol. 9, no. 8, p. 824, Aug. 2017.

[3] P. Doherty and P. Rudol, "A UAV search and rescue scenario with human body detection and geolocalization," in *Proc. Australas. Joint Conf. Artif. Intell.* Berlin, Germany: Springer, 2007, pp. 1–13.

[4] A. Puri, "A survey of unmanned aerial vehicles UAV for traffic surveillance," Dept. Comput. Sci. Eng., Univ. South Florida, Tampa, FL, USA, 2005, pp. 1–29.

[5] M. M. Ferdaus, S. G. Anavatti, M. Pratama, and M. A. Garratt, "Towards the use of fuzzy logic systems in rotary wing unmanned aerial vehicle: A review," *Artif. Intell. Rev.*, vol. 53, no. 1, pp. 1–34, 2018.

[6] A. Al-Mahturi, F. Santoso, M. A. Garratt, and S. G. Anavatti, "Online system identification for nonlinear uncertain dynamical systems using recursive interval type-2 TS fuzzy C-means clustering," in *Proc. IEEE Symp. Ser. Comput. Intell. (SSCI)*, 2020, pp. 1695–1701, doi: 10.1109/SSCI47803.2020.9308202.

[7] F. Santoso, M. A. Garratt, and S. G. Anavatti, "State-of-the-art intelligent flight control systems in unmanned aerial vehicles," *IEEE Trans. Autom. Sci. Eng.*, vol. 15, no. 2, pp. 613–627, Feb. 2017.

[8] V. P. Tran, F. Santoso, M. A. Garratt, and I. R. Petersen, "Adaptive second-order strictly negative imaginary controllers based on the interval type-2 fuzzy self-tuning systems for a hovering quadrotor with uncertainties," *IEEE/ASME Trans. Mechatronics*, vol. 25, no. 1, pp. 11–20, Feb. 2020.

[9] A. Al-Mahturi, F. Santoso, M. A. Garratt, and S. G. Anavatti, "Nonlinear altitude control of a quadcopter drone using interval type-2 fuzzy logic," in *Proc. IEEE Symp. Ser. Comput. Intell. (SSCI)*, Nov. 2018, pp. 236–241.

[10] A. Eltayeb, M. F. Rahmat, M. A. M. Basri, M. A. M. Eltoum, and S. El-Ferik, "An improved design of an adaptive sliding mode controller for chattering attenuation and trajectory tracking of the quadcopter UAV," *IEEE Access*, vol. 8, pp. 205968–205979, 2020.

[11] F. Santoso, M. A. Garratt, and S. G. Anavatti, "Fuzzy logic-based self-tuning autopilots for trajectory tracking of a low-cost quadcopter: A comparative study," in *Proc. Int. Conf. Adv. Mechatronics, Intell. Manuf., Ind. Autom. (ICAMIMIA)*, Oct. 2015, pp. 64–69.

[12] A. Al-Mahturi, F. Santoso, M. A. Garratt, and S. G. Anavatti, "Modeling and control of a quadrotor unmanned aerial vehicle using type-2 fuzzy systems," in *Unmanned Aerial Systems* (Advances in Nonlinear Dynamics and Chaos), A. Koubaa and A. T. Azar, Eds. New York, NY, USA: Academic, 2021, ch. 2, pp. 25–46. [Online]. Available: https://www.sciencedirect.com/science/article/pii/B9780128202760000091

[13] B. Xu and X. Lu, "An online adaptive control strategy for trajectory tracking of quadrotors based on fuzzy approximation and robust sliding mode algorithm," *IEEE Access*, vol. 8, pp. 215327–215342, 2020.

[14] A. Al-Mahturi, F. Santoso, M. A. Garratt, and S. G. Anavatti, "A robust self-adaptive interval type-2 TS fuzzy logic for controlling multi-input-multi-output nonlinear uncertain dynamical systems," *IEEE Trans. Syst., Man, Cybern. Syst.*, early access, Nov. 2, 2020, doi: 10.1109/TSMC.2020.3030078.

[15] A. L. Salih, M. Moghavvemi, M. A. F. Haf, and K. Gaeid, "Flight PID controller design for a UAV quadrotor," *Sci. Res. Essays*, vol. 5, pp. 3660–3667, Dec. 2010.

[16] S. Bouabdallah, A. Noth, and R. Siegwart, "PID vs LQ control techniques applied to an indoor micro quadrotor," in *Proc. IEEE/RSJ Int. Conf. Intell. Robots Syst. (IROS)*, Sep. 2004, pp. 2451–2456.

[17] K. Alexis, G. Nikolakopoulos, and A. Tzes, "Model predictive quadrotor control: Attitude, altitude and position experimental studies," *IET, Control Theory Appl.*, vol. 6, no. 12, pp. 1812–1827, Aug. 2012.

[18] H. Hagras, "Type-2 FLCs: A new generation of fuzzy controllers," *IEEE Comput. Intell. Mag.*, vol. 2, no. 1, pp. 30–43, Feb. 2007.

[19] A. Sarabakha, C. Fu, E. Kayacan, and T. Kumbasar, "Type-2 fuzzy logic controllers made even simpler: From design to deployment for UAVs," *IEEE Trans. Ind. Electron.*, vol. 65, no. 6, pp. 5069–5077, Jun. 2018.

[20] A. Matus-Vargas, G. Rodriguez-Gomez, and J. Martinez-Carranza, "Ground effect on rotorcraft unmanned aerial vehicles: A review," *Intell. Service Robot.*, vol. 14, pp. 99–118, 2021, doi: 10.1007/s11370-020-00344-5.

[21] F. Santoso, M. A. Garratt, S. G. Anavatti, and J. Wang, "Evolutionary aerial robotics: The human way of learning," in *Unmanned Aerial Systems* (Advances in Nonlinear Dynamics and Chaos), A. Koubaa and A. T. Azar, Eds. New York, NY, USA: Academic, 2021, ch. 1, pp. 1–23. [Online]. Available: https://www.sciencedirect.com/science/article/pii/B978012820276000008X

[22] A. Al-Mahturi, F. Santoso, M. A. Garratt, and S. G. Anavatti, "An intelligent control of an inverted pendulum based on an adaptive interval type-2 fuzzy inference system," in *Proc. IEEE Int. Conf. Fuzzy Syst. (FUZZ-IEEE)*, 2019, pp. 1–6, doi: 10.1109/FUZZ-IEEE.2019.8858948.

[23] L.-X. Xu, H.-J. Ma, D. Guo, A.-H. Xie, and D.-L. Song, "Backstepping sliding-mode and cascade active disturbance rejection control for a quadrotor UAV," *IEEE/ASME Trans. Mechatronics*, vol. 25, no. 6, pp. 2743–2753, Dec. 2020.

[24] H. Yin, W. Zhou, M. Li, C. Ma, and C. Zhao, "An adaptive fuzzy logic-based energy management strategy on battery/ultracapacitor hybrid electric vehicles," *IEEE Trans. Transport. Electrific.*, vol. 2, no. 3, pp. 300–311, Sep. 2016.

[25] J. Zhang, X. Wang, and X. Shao, "Design and real-time implementation of Takagi–Sugeno fuzzy controller for magnetic levitation ball system," *IEEE Access*, vol. 8, pp. 38221–38228, 2020.

[26] O. Castillo and P. Melin, "A review on interval type-2 fuzzy logic applications in intelligent control," *Inf. Sci.*, vol. 279, pp. 615–631, Sep. 2014. [Online]. Available: http://linkinghub.elsevier.com/retrieve/pii/S0020025514004629

[27] A. J. Al-Mahasneh, S. G. Anavatti, M. A. Garratt, and M. Pratama, "Stable adaptive controller based on generalized regression neural networks and sliding mode control for a class of nonlinear time-varying systems," *IEEE Trans. Syst., Man, Cybern., Syst.*, vol. 51, no. 4, pp. 2525–2535, Apr. 2019.

[28] M. M. Ferdaus, M. Pratama, S. G. Anavatti, M. A. Garratt, and Y. Pan, "Generic evolving self-organizing neuro-fuzzy control of bio-inspired unmanned aerial vehicles," *IEEE Trans. Fuzzy Syst.*, vol. 28, no. 8, pp. 1542–1556, Aug. 2020.

[29] R.-J. Wai and A. S. Prasetia, "Adaptive neural network control and optimal path planning of UAV surveillance system with energy consumption prediction," *IEEE Access*, vol. 7, pp. 126137–126153, 2019.

[30] A. Al-Mahturi, F. Santoso, M. A. Garratt, and S. G. Anavatti, "A robust adaptive interval type-2 fuzzy control for autonomous underwater vehicles," in *Proc. IEEE Int. Conf. Ind. 4.0, Artif. Intell., Commun. Technol. (IAICT)*, Jul. 2019, pp. 19–24.

[31] A. Al-Mahturi, F. Santoso, M. A. Garratt, S. G. Anavatti, and M. M. Ferdaus, "Online takagi-sugeno fuzzy identification of a quadcopter using experimental input-output data," in *Proc. IEEE Symp. Ser. Comput. Intell. (SSCI)*, Dec. 2019, pp. 527–533.

[32] Y. Zhao, J. Wang, F. Yan, and Y. Shen, "Adaptive sliding mode fault-tolerant control for type-2 fuzzy systems with distributed delays," *Inf. Sci.*, vol. 473, pp. 227–238, Jan. 2019. [Online]. Available: http://www.sciencedirect.com/science/article/pii/S0020025518306911

[33] A. Al-Mahturi, F. Santoso, M. A. Garratt, and S. G. Anavatti, "A simplified model-free self-evolving TS fuzzy controller for nonlinear systems with uncertainties," in *Proc. IEEE Conf. Evolving Adapt. Intell. Syst. (EAIS)*, May 2020, pp. 1–6.

[34] J. M. Mendel, *Uncertain Rule-Based Fuzzy Systems: Introduction and New Directions*. Cham, Switzerland: Springer, 2019.

[35] Q. Lu, P. Shi, H.-K. Lam, and Y. Zhao, "Interval type-2 fuzzy model predictive control of nonlinear networked control systems," *IEEE Trans. Fuzzy Syst.*, vol. 23, no. 6, pp. 2317–2328, Dec. 2015.

[36] J. M. Mendel, R. I. John, and F. Liu, "Interval type-2 fuzzy logic systems made simple," *IEEE Trans. Fuzzy Syst.*, vol. 14, no. 6, pp. 808–821, Dec. 2006.

[37] T.-L. Le, N. V. Quynh, N. K. Long, and S. K. Hong, "Multilayer interval type-2 fuzzy controller design for quadcopter unmanned aerial vehicles using Jaya algorithm," *IEEE Access*, vol. 8, pp. 181246–181257, 2020.

[38] D. Wu, "Approaches for reducing the computational cost of interval type-2 fuzzy logic systems: Overview and comparisons," *IEEE Trans. Fuzzy Syst.*, vol. 21, no. 1, pp. 80–99, Feb. 2012.

[39] M. Nie and W. W. Tan, "Towards an efficient type-reduction method for interval type-2 fuzzy logic systems," in *Proc. IEEE Int. Conf. Fuzzy Syst. (FUZZ-IEEE)*, Jun. 2008, pp. 1425–1432.

[40] T.-T. Huynh, C.-M. Lin, T.-L. Le, H.-Y. Cho, T.-T.-T. Pham, N.-Q.-K. Le, and F. Chao, "A new self-organizing fuzzy cerebellar model articulation controller for uncertain nonlinear systems using overlapped Gaussian membership functions," *IEEE Trans. Ind. Electron.*, vol. 67, no. 11, pp. 9671–9682, Nov. 2020.

[41] E. Kayacan and R. Maslim, "Type-2 fuzzy logic trajectory tracking control of quadrotor VTOL aircraft with elliptic membership functions," *IEEE/ASME Trans. Mechatronics*, vol. 22, no. 1, pp. 339–348, Feb. 2017.

[42] H. Li, J. Wang, H.-K. Lam, Q. Zhou, and H. Du, "Adaptive sliding mode control for interval type-2 fuzzy systems," *IEEE Trans. Syst., Man, Cybern., Syst.*, vol. 46, no. 12, pp. 1654–1663, Dec. 2017.

[43] P. K. Ray, S. R. Paital, A. Mohanty, Y. S. E. Foo, A. Krishnan, H. B. Gooi, and G. A. J. Amaratunga, "A hybrid firefly-swarm optimized fractional order interval type-2 fuzzy PID-PSS for transient stability improvement," *IEEE Trans. Ind. Appl.*, vol. 55, no. 6, pp. 6486–6498, Nov. 2019.

[44] S. Zeghlache, K. Kara, and D. Saigaa, "Fault tolerant control based on interval type-2 fuzzy sliding mode controller for coaxial trirotor aircraft," *ISA Trans.*, vol. 59, pp. 215–231, Nov. 2015. [Online]. Available: http://linkinghub.elsevier.com/retrieve/pii/S0019057815002207
[45] C. Li, G. Zhang, J. Yi, and M. Wang, "Uncertainty degree and modeling of interval type-2 fuzzy sets: Definition, method and application," *Comput. Math. Appl.*, vol. 66, no. 10, pp. 1822–1835, Dec. 2013.
[46] S. Bouabdallah, "Design and control of quadrotors with application to autonomous flying," EPFL, Lausanne, Switzerland, Tech. Rep., 2007. [Online]. Available: https://infoscience.epfl.ch/record/95939
[47] J. Lin, R.-J. Lian, C.-N. Huang, and W.-T. Sie, "Enhanced fuzzy sliding mode controller for active suspension systems," *Mechatronics*, vol. 19, no. 7, pp. 1178–1190, Oct. 2009.
[48] S.-J. Huang and W.-C. Lin, "Adaptive fuzzy controller with sliding surface for vehicle suspension control," *IEEE Trans. Fuzzy Syst.*, vol. 11, no. 4, pp. 550–559, Aug. 2003.
[49] A. Saghafinia, H. W. Ping, M. N. Uddin, and K. S. Gaeid, "Adaptive fuzzy sliding-mode control into chattering-free IM drive," *IEEE Trans. Ind. Appl.*, vol. 51, no. 1, pp. 692–701, Jan./Feb. 2014.
[50] A. J. Al-Mahasneh, S. G. Anavatti, and M. A. Garratt, "Self-evolving neural control for a class of nonlinear discrete-time dynamic systems with unknown dynamics and unknown disturbances," *IEEE Trans. Ind. Informat.*, vol. 16, no. 10, pp. 6518–6529, Oct. 2020.
[51] R.-J. Lian, "Enhanced adaptive self-organizing fuzzy sliding-mode controller for active suspension systems," *IEEE Trans. Ind. Electron.*, vol. 60, no. 3, pp. 958–968, Mar. 2013.
[52] K. S. Narendra and A. M. Annaswamy, "A new adaptive law for robust adaptation without persistent excitation," in *Proc. Amer. Control Conf.*, Jun. 1986, pp. 1067–1072.
[53] F.-C. Chen and H. K. Khalil, "Adaptive control of nonlinear systems using neural networks—A dead-zone approach," in *Proc. Amer. Control Conf.*, Jun. 1991, pp. 667–672.

AYAD AL-MAHTURI (Student Member, IEEE) received the B.E. degree in mechatronics engineering from IIUM, Malaysia, in 2015, and the M.Sc. degree in mechatronics and automatic control engineering from the University of Technology, Malaysia, in 2017. He is currently pursuing the Ph.D. degree with the University of New South Wales (UNSW), Australia. He received the Best Postgraduate Student Award as well as the Pro-Chancellor Award during his master's degree. He served as the IEEE Student Branch Representative at UNSW, in 2019. His current research interests include fuzzy systems, modeling and control of nonlinear dynamic systems such as unmanned aerial vehicles, and robotics. He has been a Reviewer for multiple high-impact journals, such as IEEE TRANSACTIONS ON SYSTEMS, MAN, AND CYBERNETICS: SYSTEMS, IEEE/ASME TRANSACTIONS ON MECHATRONICS, *Information Sciences*, and IEEE ACCESS.

FENDY SANTOSO (Senior Member, IEEE) received the master's degree in electrical and computer systems engineering from Monash University, Melbourne, VIC, Australia, in 2007, and the Ph.D. degree in electrical engineering from the University of New South Wales (UNSW), Sydney, NSW, Australia, in 2012. Prior to joining the Defence and Systems Institute (DASI), Science, Technology, Engineering, and Mathematics (STEM), University of South Australia, Mawson Lakes, Adelaide, SA, Australia, as a Research Fellow, he was with the School of Engineering and Information Technology, UNSW, Canberra, ACT, Australia, as a Research Fellow. His current research interests include control systems and artificial intelligence with applications in aerial robotics. He is an Associate Editor of the *International Journal of Knowledge-Based and Intelligent Engineering Systems*. He has been a Reviewer for multiple high-impact control and robotics journals, such as IEEE TRANSACTIONS ON FUZZY SYSTEMS, IEEE TRANSACTIONS ON SYSTEMS, MAN, AND CYBERNETICS: SYSTEMS, IEEE ROBOTICS AND AUTOMATION LETTERS (RAL), and IEEE TRANSACTIONS ON NEURAL NETWORKS AND LEARNING SYSTEMS, in addition to many international conferences.

MATTHEW A. GARRATT (Senior Member, IEEE) received the B.E. degree in aeronautical engineering from The University of Sydney, Camperdown, NSW, Australia, in 1990, the Graduate Diploma degree in applied computer science from Central Queensland University, Rockhampton, QLD, Australia, in 1997, and the Ph.D. degree in the field of biologically inspired robotics from The Australian National University, Canberra, ACT, Australia, in 2008. He is currently a Professor with the School of Engineering and Information Technology (SEIT), University of New South Wales, Canberra. His research interests include sensing, guidance, and control for autonomous systems with particular emphasis on biologically inspired and computational intelligence approaches. He is also the Chair of the CIS task force on the ethics and social implications of CI. He is an Associate Editor of the IEEE TRANSACTIONS ON ARTIFICIAL INTELLIGENCE.

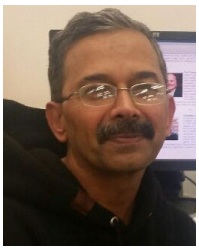

SREENATHA G. ANAVATTI received the B.E. degree in mechanical engineering from the University of Mysore, Mysuru, Karnataka, India, in 1984, and the Ph.D. degree in aerospace engineering from the Indian Institute of Science, Bengaluru, India, in 1990. He is currently a Senior Lecturer with the School of Engineering and Information Technology, University of New South Wales, Canberra, ACT, Australia. He moved to Australia, in 1998. Before that, he was with the Indian Institute of Technology Bombay, Mumbai, India, as an Associate Professor. He has supervised a number of Ph.D. scholars over these years. His research interests include application of artificial intelligence techniques, such as fuzzy and neural systems for UAVs, underwater vehicles, ground vehicles, identification and control of dynamic systems, navigation and path planning for autonomous vehicles, evolutionary fuzzy systems, and their applications to dynamic systems.